237497: andalusite–cordierite pelitic schist, Sunbeam pit

(Youanmi Terrane, Yilgarn Craton)

Korhonen, FJ, Kelsey DE and Ivanic, TJ

Location and sampling

Southern Cross (SH 50-16), Southern Cross (2735)

MGA Zone 50, 721635E 6536715N

Warox Site JRLSCD000011

Sampled on 27 June 2018

This sample was collected from the 430.5 – 430.8 m depth interval of diamond drillhole JPDD02, drilled in 2015 by Hanking Gold Mining at their Jupiter project (Xue, 2015), and co-funded under the Exploration Incentive Scheme (EIS). The drillhole is located about 5.5 km south of Southern Cross townsite, 2.5 km west of the Southern Cross – Marvel Loch Road, and 0.1 km east of the Sunbeam pit.

Geological context

The unit sampled is a pelitic schist in the Southern Cross greenstone belt of the Youanmi Terrane (Doublier, 2012, 2013; Doublier et al., 2014). The Southern Cross belt consists of a lower tholeiitic and komatiitic metavolcanic succession, up to 5 km thick, overlain by at least 2 km of clastic metasedimentary rocks (Doublier, 2013). Detrital zircons in a metasedimentary sample about 0.6 km to the north yielded a conservative maximum depositional age of 2675 ± 8 Ma (GSWA 205918, Thébaud et al., 2014). The sample reported here preserves two monazite age components that can be differentiated based on petrographic setting: Group M monazite occurs within andalusite porphyroblasts and in plagioclase–biotite–quartz intergrowths replacing andalusite, and yielded an age of 2671 ± 14 Ma; Group M2 monazite occurs within the foliated microcrystalline matrix and in cordierite porphyroblasts, and yielded an age of 2629 ± 9 Ma (GSWA 237497, Fielding et al., 2021). A sample of garnet-bearing pelitic gneiss collected from the same drillhole as the sample reported here yielded peak *P–T* estimates of 2.4 – 3.5 kbar and 575–655 °C (GSWA 237496, preliminary data), and a monazite age of c. 2622 Ma (GSWA 237496, preliminary data).
A summary of the metamorphic evolution of the southwest Yilgarn is provided in Korhonen et al. (2021).

Petrographic description

The sample is a pelitic schist consisting of about 25% biotite, 20–25% cordierite, 10–15% plagioclase, 10–15% quartz, 10% graphite, 8% andalusite, 3% muscovite, 2% chlorite, 1% pyrrhotite and accessory apatite, monazite and ilmenite (Fig. 1; Table 1). Porphyroblasts of andalusite and poikiloblasts of cordierite occur within a matrix of microcrystalline quartz and graphite and coarser grained biotite and minor muscovite that define a weak to moderate foliation. Biotite is anhedral, up to 1.5 mm long, and contains rounded inclusions of plagioclase. Muscovite is typically less than 0.5 mm long with ragged grain edges. Rounded aggregates of plagioclase up to 0.5 mm in diameter occur as inclusions in biotite and within the quartz–graphite matrix (Fig. 2a). Biotite, muscovite and plagioclase within the matrix are riddled with very fine-grained (<<100 µm) graphite. Euhedral andalusite porphyroblasts are up to 1 cm long and contain rare, small and rounded inclusions of plagioclase, pyrrhotite, muscovite and biotite (Fig. 1). The margins of andalusite porphyroblasts are in contact with distinct domains of intergrown graphite-free plagioclase, biotite and quartz that penetrate into the cores (Fig. 2c,d). Andalusite grain boundaries adjacent to these plagioclase–biotite–quartz intergrowths are embayed. Cordierite occurs in some of these domains, possibly truncating biotite laths (Fig. 2e). Cordierite poikiloblasts are anhedral, up to 2 cm in diameter; the inclusions within cordierite are the same minerals as those in the foliated matrix (Fig. 2b).

Some cordierite poikiloblasts contain rare, small grains of embayed and elongate andalusite up to 500 µm in length. These grains are closely associated with rounded inclusion-free biotite and mantled by inclusion-free cordierite that is in optical continuity with the graphite-rich poikiloblasts (Fig. 2f). Coarse-grained muscovite and chlorite are common on the margins of andalusite and cordierite porphyroblasts. Pyrrhotite occurs as rounded and elongate grains aligned with the foliation and occurs within the matrix, as elongate clasts intergrown with polycrystalline quartz, and as inclusions in most of the minerals including quartz, cordierite, biotite, andalusite and Group M monazite.

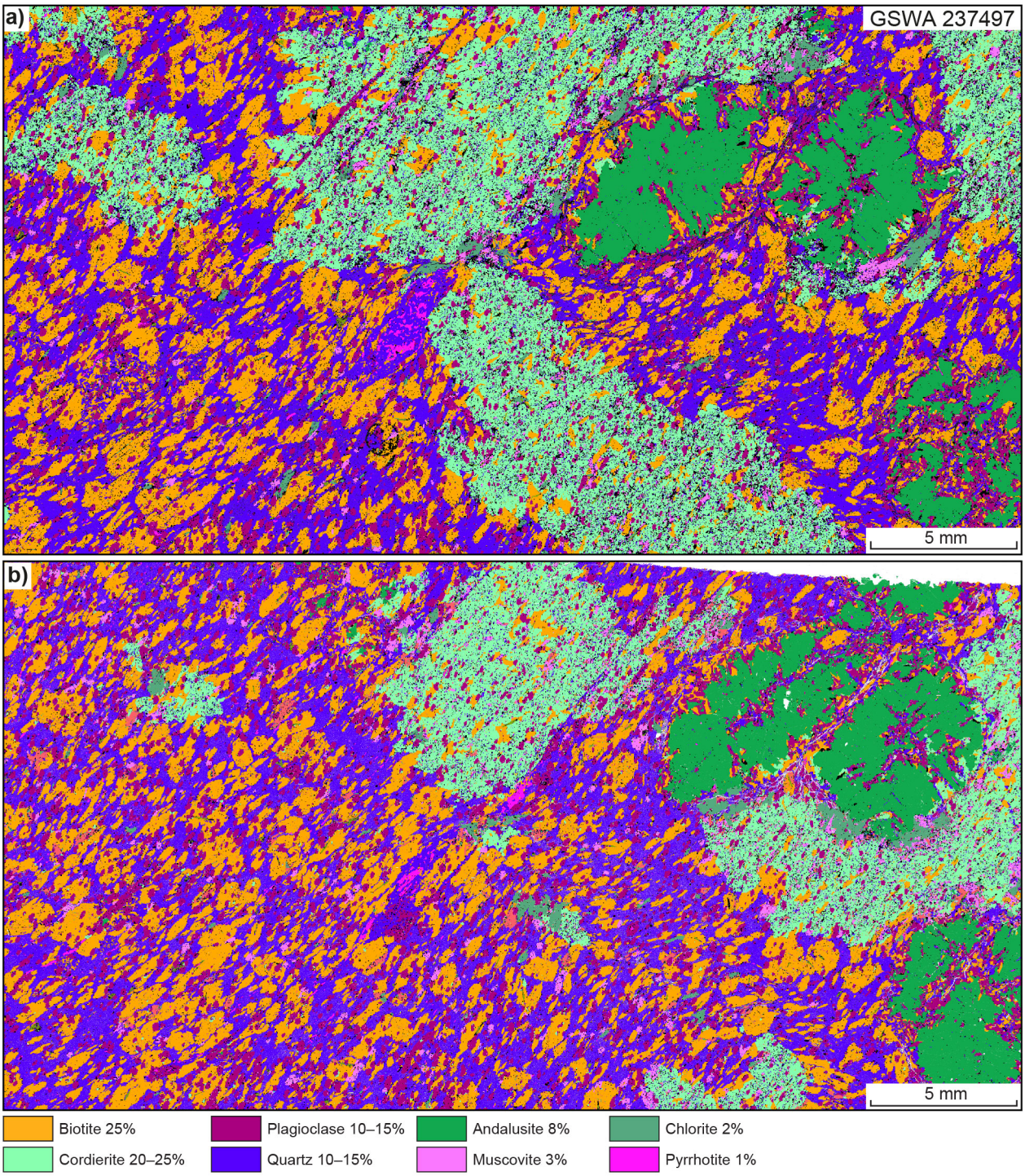

Figure 1. **TESCAN Integrated Mineral Analyser (TIMA) image of two entire thin sections (a, b) from sample 237497: andalusite–cordierite pelitic schist, Sunbeam pit. Thin sections were prepared from the same rock billet. Volume percent proportions of major rock-forming minerals are calculated by the TIMA software**

Table 1. Mineral modes for sample 237497: cordierite–andalusite pelitic schist, Sunbeam pit

Mineral modes	*Bt*	*Crd*	*Pl*	*Qz*	*And*	*Ilm*	*Ms*	*Chl*	*Gr*
Observed (vol%)	25	20–25	10–15	10–15	8	<1	3	2	10
Predicted (mol%)									
@ 2 kbar, 575 °C	24.8	20.9	16.3	30.2	7.1	0.7	–	–	–
@ 2 kbar, 625 °C	24.5	22.6	16.4	29.8	6.0	0.6	–	–	–

NOTES: – not present

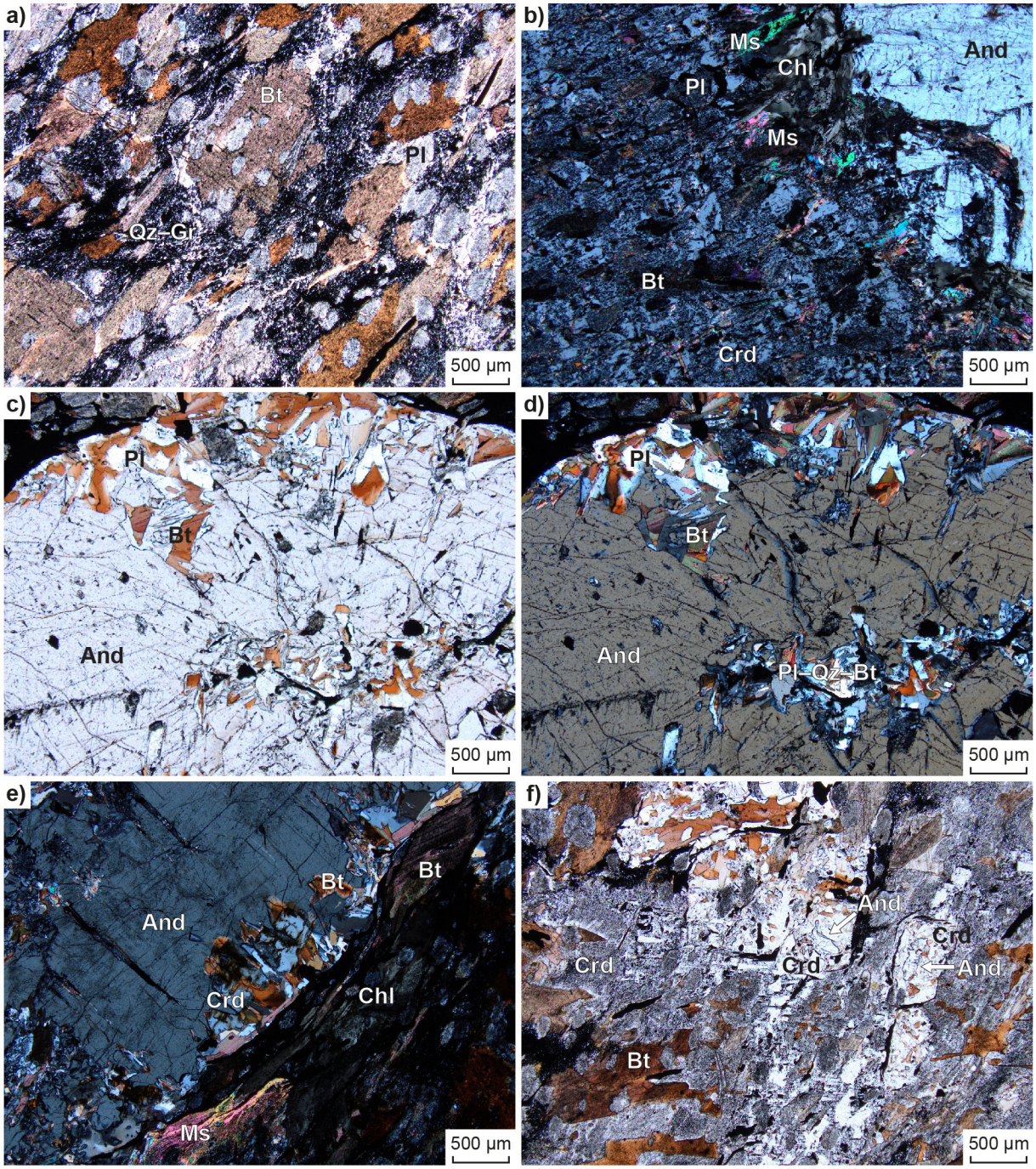

Figure 2. **Photomicrographs, in plane-polarized light (a, c, f) and cross-polarized light (b, d, e), of sample 237497: andalusite–cordierite pelitic schist, Sunbeam pit. Mineral abbreviations are explained in the caption to Figure 3, except Gr, graphite**

Analytical details

The metamorphic evolution of this sample was investigated using phase equilibria, based on the bulk-rock composition (Table 2). The composition was determined by X-ray fluorescence spectroscopy, together with loss on ignition (LOI). FeO content was analysed by Fe^{2+} titration, and Fe_2O_3 calculated by difference. The modelled O content (for Fe^{3+}) was derived from the titration value. The subsolidus mineral assemblages are assumed to have equilibrated in the presence of a pure H_2O volatile fluid; therefore, the calculations were performed in an H_2O-saturated system. The bulk composition was adjusted for the presence of apatite by applying a correction to CaO, and pyrrhotite by applying a correction to FeO (Table 2). Thermodynamic calculations were performed in the MnNCKFMASHTO ($MnO–Na_2O–CaO–K_2O–FeO–MgO–Al_2O_3–SiO_2–H_2O–TiO_2–O$) system using THERMOCALC version tc340 (updated October 2013; Powell and Holland, 1988) and the internally consistent thermodynamic dataset of Holland and Powell (2011; dataset tc-ds62, created in February 2012). The activity–composition relations used in the modelling are detailed in White et al. (2014a,b). Compositional and mode isopleths for all phases were calculated using the software TCInvestigator (Pearce et al., 2015). Additional information on the workflow with relevant background and methodology are provided in Korhonen et al. (2020).

Table 2. Measured whole-rock and modelled compositions for sample 237497: cordierite–andalusite pelitic schist, Sunbeam pit

XRF whole-rock composition (wt%)[a]

SiO_2	TiO_2	Al_2O_3	Fe_2O_3	FeO[b]	MnO	MgO	CaO	Na_2O	K_2O	P_2O_5	SO_3	LOI	Total
56.45	0.85	19.58	0.54	8.60	0.15	4.29	1.83	0.82	2.48	0.08	2.20	3.41	101.28

Normalized composition used for phase equilibria modelling (mol%); Figure 4

SiO_2	TiO_2	Al_2O_3	O[c]	FeO^T[d]	MnO	MgO	CaO[e]	Na_2O	K_2O	–		H_2O[f]	Total
65.99	0.75	13.49	0.24	6.95	0.15	7.48	2.17	0.93	1.85	--	--	excess	100

Normalized composition used for phase equilibria modelling (mol%)[g]

SiO_2	TiO_2	Al_2O_3	O	FeO^T	MnO	MgO	CaO	Na_2O	K_2O	–		H_2O	Total
66.74	0.78	11.79	0.25	7.27	0.16	7.83	2.27	0.97	1.94	--	--	excess	100

NOTES:
(a) Data and analytical details are available from the WACHEM database <http://geochem.dmp.wa.gov.au/geochem/>
(b) FeO analysed by Fe^{2+} titration; Fe_2O_3 content calculated by difference
(c) O content (for Fe_2O_3) derived from the titration value
(d) FeO^T = moles FeO + 2 * moles O. Also modified to remove pyrrhotite = moles FeO^T - moles SO_2
(e) CaO modified to remove apatite: CaO(Mod) = CaO(Total) - (moles CaO(in Ap) = 3.33 * moles P_2O_5)
(f) H_2O-saturated
(g) calculated using modes and compositions at 2 kbar, 600 °C from Figure 3

Results

Metamorphic *P–T* estimates have been derived based on detailed examination of two thin sections and a single bulk-rock composition. Care was taken to ensure that the thin sections and the sample volume selected for whole-rock chemistry were similar in terms of featuring the same minerals in approximately the same abundances (Table 1), to minimize any potential compositional differences. The *P–T* pseudosection for sample 237497 was calculated over a *P–T* range of 0.5 – 4 kbar and 500–700 °C (Fig. 3). The H_2O-saturated solidus has a minimum stability of 690 °C at 3.2 kbar over the modelled *P–T* range. Cordierite is stable across most of the range of modelled conditions, except at lower temperatures where chlorite is stable. Within cordierite-bearing assemblages, andalusite is not stable at low pressure and high temperature. Garnet is stable above 0.9 kbar at 500 °C and above 3.4 kbar at 695 °C. K-feldspar is stable below 0.5 kbar at 540 °C and below 3.2 kbar at 690 °C.

Interpretation

Based on the microstructural observations and the monazite ages, the sample may preserve evidence for a polymetamorphic evolution. The growth of cordierite occurred at the expense of andalusite, although it is difficult to resolve whether this sequence of growth occurred during the same event or two separate events. Monazite inclusions in the andalusite porphyroblasts and in the plagioclase–biotite–quartz±cordierite intergrowths that replace andalusite yielded an age of 2671 ± 14 Ma (Group M). One possibility is that this age dates the timing of andalusite growth; a second interpretation is that the andalusite overgrew

pre-existing monazite and is younger than the Group M monazite age. Monazite within the foliated matrix and in cordierite porphyroblasts that overgrew the foliated matrix yielded an age of 2629 ± 9 Ma (Group M2), which is interpreted to date the timing of cordierite growth. The presence of pyrrhotite inclusions in andalusite and in Group M monazite indicates that sulfide mineralization predates the c. 2671 Ma event.

The peak metamorphic assemblage includes cordierite, which in the pseudosection is predicted to be stable with garnet–andalusite at higher pressures, followed by andalusite-, andalusite–K-feldspar-, and K-feldspar-bearing assemblages with decreasing pressure (Fig. 3). There is no evidence for the stability of garnet or K-feldspar in the sample, which implies that the peak assemblage likely included andalusite. In this interpretation, the inferred peak assemblage of cordierite–biotite–andalusite–plagioclase–ilmenite–quartz–H_2O has a maximum pressure stability of 3 kbar between 500 and 670 °C. The predicted mineral modes (molar proportions approximately equivalent to vol%) across the peak field at 2 kbar are broadly similar to the modes observed in the thin section (Table 1). The peak field is delimited by the stability of garnet at higher pressure and lower temperature, and the stability of K-feldspar at lower pressure and higher temperature. Modal isopleths for andalusite and cordierite have inclined slopes across the peak field, and cordierite modes increase slightly at the expense of andalusite with increasing temperature, with or without an increase in pressure (Fig. 4). This trajectory implies that at least some andalusite was in equilibrium with cordierite at c. 2629 Ma.

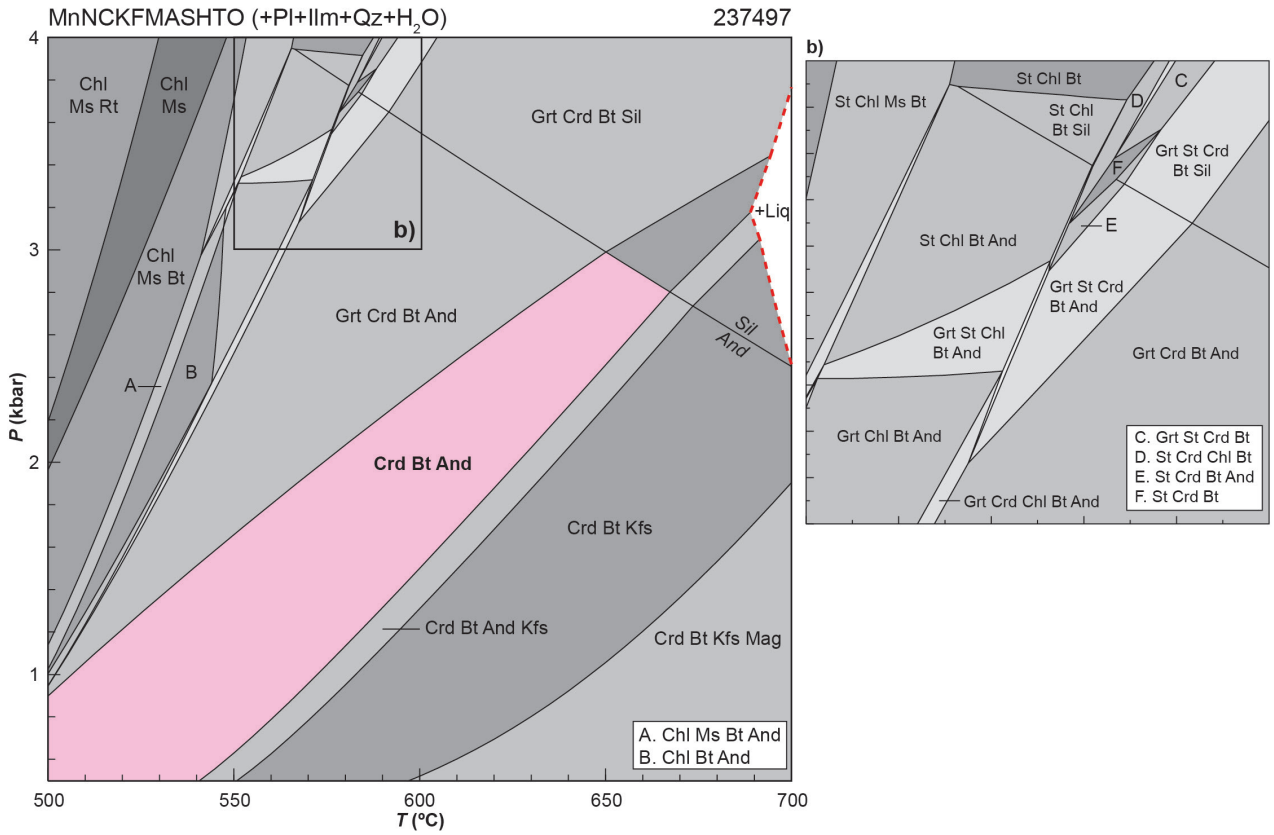

Figure 3. ***P–T*** **pseudosection calculated for sample 237497: cordierite–andalusite pelitic schist, Sunbeam pit. Assemblage fields corresponding to peak metamorphic conditions are delimited by bold text and pink shading. Red dashed line represents the solidus. Abbreviations: And, andalusite; Bt, biotite; Chl, chlorite; Crd, cordierite; Grt, garnet; H_2O, fluid (pure H_2O); Ilm, ilmenite; Kfs, K-feldspar; Liq, silicate melt; Mag, magnetite; Ms, muscovite; Pl, plagioclase; Qz, quartz; Rt, rutile; St, staurolite**

It is also possible that andalusite, but not cordierite, was part of an older metamorphic assemblage, as suggested by the c. 2671 Ma Group M monazite age. Andalusite in the absence of cordierite and garnet has a narrow stability between 1.1 and 3.2 kbar at 500–550 °C (fields A, B on Figure 3), and the presence of biotite and muscovite inclusions in andalusite is consistent with these conditions. In this model, andalusite porphyroblasts may have been metastable with respect to cordierite in a later, overprinting event and therefore not (fully) part of the equilibration volume represented by the modelled bulk-rock composition. To investigate this possibility, a second *P–T* pseudosection was calculated (not shown), with the bulk composition derived by removal of most andalusite. A small amount of andalusite (1 mol%; Table 2) was retained in order to simulate the interaction of its grain edges with the equilibration volume. Although this changes the bulk composition slightly (Table 2), the topology of the calculated pseudosection is identical to Figure 3; the only differences are very minor variations in the mineral modes and compositions. These results suggest that at least some andalusite must have been in equilibrium with cordierite at peak conditions. The subsequent breakdown of andalusite is most consistent with an increase in temperature within the peak assemblage field (Fig. 4). The absence of garnet and K-feldspar in the sample implies a relatively tight *P–T* trajectory within the Crd–Bt–And (+Pl+Ilm+Qz+H_2O) field, although the possibility that the prograde path passed through the stability fields for these phases and were completely consumed cannot be unequivocally ruled out.

Maximum peak metamorphic conditions are estimated at 670 °C and 3 kbar at c. 2629 Ma, with a minimum apparent thermal gradient of 225 °C/kbar. These conditions occur within the ultrahigh *T/P* thermal regime (see Korhonen et al., 2020) and are consistent with regional contact metamorphism related to the emplacement of voluminous granitic rocks across the Yilgarn Craton at this time. Andalusite may record an earlier metamorphic event (at c. 2671 Ma?) with conditions estimated at 1.1 – 3.2 kbar and 500–550 °C, although it may also record prograde conditions of the c. 2629 Ma event. The preserved assemblage is most consistent with a tight *P–T* trajectory. These *P–T* conditions are closely comparable to those of 2.4 – 3.5 kbar and 575–655 °C from garnet-bearing sample GSWA 237496 (preliminary data) from the same drillcore.

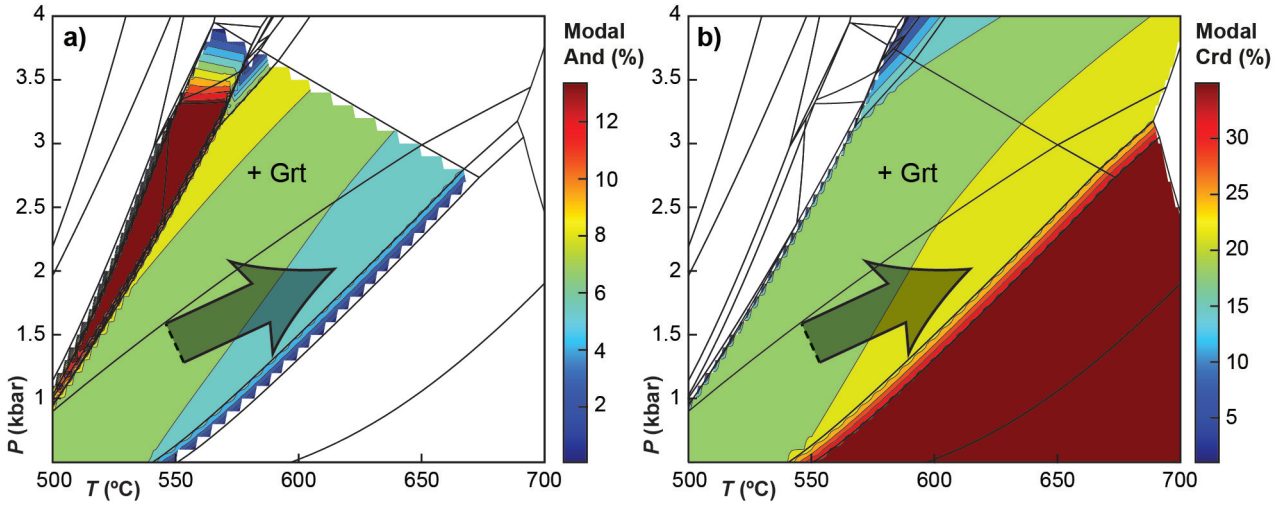

Figure 4. **Calculated modes (%) for the *P–T* pseudosections for sample 237497: cordierite–andalusite pelitic schist, Sunbeam pit: a) Modal proportions (approximately equal to volume percent) for andalusite; b) mode isopleths for cordierite. The mode increase of cordierite at the expense of andalusite occurs with increasing temperature with or without an increase in pressure; schematic *P–T* path within the peak field is represented by the grey arrow, with thickness of the arrow to qualitatively depict uncertainty. The *P–T* path depicts approximate trajectory, not absolute conditions. See Figure 3 for labelled *P–T* diagram**

References

Doublier, MP 2012, Southern Cross, WA sheet 2735: Geological Survey of Western Australia, 1:100 000 Geological Series.

Doublier, MP (compiler) 2013, Geological setting of mineral deposits in the Southern Cross district — a field guide: Geological Survey of Western Australia, Record 2013/11, 55p.

Doublier, MP, Thébaud, N, Wingate, MTD, Romano, SS, Kirkland, CL, Gessner, K, Mole, DR and Evans, N 2014, Structure and timing of Neoarchean gold mineralization in the Southern Cross district (Yilgarn Craton, Western Australia) suggest leading role of late low- Ca I-type granite intrusions: Journal of Structural Geology, v. 67, p. 205–221.

Fielding, IOH, Wingate, MTD, Lu, Y, Korhonen, FJ and Rankenburg, K 2021, 237497: pelitic gneiss, Sunbeam pit; Geochronology Record 1773: Geological Survey of Western Australia, 5p.

Holland, TJB and Powell, R 2011, An improved and extended internally consistent thermodynamic dataset for phases of petrological interest, involving a new equation of state for solids: Journal of Metamorphic Geology, v. 29, no. 3, p. 333–383.

Korhonen, FJ, Blereau, ER, Kelsey, DE, Fielding, IOH and Romano, SS 2021, Metamorphic evolution of the southwest Yilgarn, *in* Accelerated Geoscience Program: extended: Geological Survey of Western Australia Record 2021/4, p. 108–115.

Korhonen, FJ, Kelsey, DE, Fielding IOH and Romano, SS 2020, The utility of the metamorphic rock record: constraining the pressure–temperature–time conditions of metamorphism: Geological Survey of Western Australia, Record 2020/14, 24p.

Pearce, MA, White, AJR and Gazley, MF 2015, TCInvestigator: automated calculation of mineral mode and composition contours for thermocalc pseudosections: Journal of Metamorphic Geology, v. 33, no. 4, p. 413–425, doi:10.1111/jmg.12126.

Powell, R and Holland, TJB 1988, An internally consistent dataset with uncertainties and correlations: 3. Applications to geobarometry, worked examples and a computer program: Journal of Metamorphic Geology, v. 6, no. 2, p. 173–204.

Thébaud, N, Mole, DM, Wingate, MTD, Kirkland, CL and Doublier, MP 2014, 205918: altered metasedimentary rock, Transvaal mine; Geochronology Record 1167: Geological Survey of Western Australia, 6p.

White, RW, Powell, R, Holland, TJB, Johnson, TE and Green, ECR 2014a, New mineral activity–composition relations for thermodynamic calculations in metapelitic systems: Journal of Metamorphic Geology, v. 32, no. 3, p. 261–286.

White, RW, Powell, R and Johnson, TE 2014b, The effect of Mn on mineral stability in metapelites revisited: New *a–x* relations for manganese-bearing minerals: Journal of Metamorphic Geology, v. 32, no. 8, p. 809–828.

Xue, G 2015, Jupiter Project Co-funded Drilling Program: Exploration Report A105859 (unpublished), 56p.

Links

Metamorphic history introduction document: Intro_2020.pdf

Recommended reference for this publication

Korhonen, FJ, Kelsey DE and Ivanic, TJ 2022, 237497: andalusite–cordierite pelitic schist, Sunbeam pit; Metamorphic History Record 19: Geological Survey of Western Australia, 8p.

Data obtained: 12 January 2022

Date released: 14 April 2022

This Metamorphic History Record was last modified on 29 March 2022.

Grid references in this publication refer to the Geocentric Datum of Australia 1994 (GDA94). All locations are quoted to at least the nearest 100 m.

WAROX is GSWA's field observation and sample database. WAROX site IDs have the format 'ABCXXXnnnnnnSS', where ABC = geologist username, XXX = project or map code, nnnnnn = 6 digit site number, and SS = optional alphabetic suffix (maximum 2 characters).

Isotope and element analyses are routinely conducted using the GeoHistory laser ablation ICP-MS and Sensitive High-Resolution Ion Microprobe (SHRIMP) ion microprobe facilities at the John de Laeter Centre (JdLC), Curtin University, with the financial support of the Australian Research Council and AuScope National Collaborative Research Infrastructure Strategy (NCRIS). The TESCAN Integrated Mineral Analyser (TIMA) instrument was funded by a grant from the Australian Research Council (LE140100150) and is operated by the JdLC with the support of the Geological Survey of Western Australia, The University of Western Australia (UWA) and Murdoch University. Mineral analyses are routinely obtained using the electron probe microanalyser (EPMA) facilities at the Centre for Microscopy, Characterisation and Analysis at UWA, and at Adelaide Microscopy, University of Adelaide.

Digital data related to WA Geology Online, including geochronology and digital geology, are available online at the Department's Data and Software Centre and may be viewed in map context at GeoVIEW.WA.

Further details of geoscience products are available from:
Information Centre
Department of Mines, Industry Regulation and Safety
100 Plain Street
EAST PERTH WA 6004
Telephone: +61 8 9222 3459 | Email: publications@dmirs.wa.gov.au
www.dmirs.wa.gov.au/GSWApublications